# NMR Characterization of Side Chain Flexibility and Backbone Structure in the Type I Antifreeze Protein at Near Freezing Temperatures[†]

Wolfram Gronwald,[‡,§] Heman Chao,[‡,§] D. Venkat Reddy,[||] Peter L. Davies,[‡,⊥] Brian D. Sykes,*[,‡,§] and Frank D. Sönnichsen[||]

*Protein Engineering Network of Centres of Excellence, University of Alberta, Edmonton, Alberta T6G 2S2, Canada, Department of Biochemistry, University of Alberta, Edmonton, Alberta T6G 2H7, Canada, Department of Physiology and Biophysics, Case Western Reserve University, Cleveland, Ohio 44106-4970, and Department of Biochemistry, Queen's University, Kingston, Ontario K7L 3N6, Canada*

*Received August 5, 1996; Revised Manuscript Received October 26, 1996*[⊗]

ABSTRACT: The flexibility of the polar side chains in the α-helical Type I antifreeze protein (AFP) near the solution freezing temperature was investigated by two-dimensional nuclear magnetic resonance spectroscopy. These experiments were conducted to define the rotameric conformations of the proposed ice-binding groups, threonines and asparagines, in order to probe the molecular mechanism for ice binding. On the basis of the $^3J_{\alpha\beta}{}^2$ NMR coupling constant values of 7.1, 8.5, 8.5, and 6.8 Hz for residues T2, T13, T24, and T35, respectively, it can be calculated that the regularly spaced ice-binding threonines sample many possible rotameric states prior to ice binding. The lack of a dominant side chain rotamer is further corroborated by nuclear Overhauser distance measurements for T13 and T24. N16 and N27, both with $^3J_{\alpha\beta}{}^2$ and $^3J_{\alpha\beta}{}^3$ coupling constants of 8.4 and 4.5 Hz, respectively, show a slight preference for the side chain conformation with a $\chi_1$ of −60°. These data suggest that prior to ice binding the threonine and asparagine side chains are free to rotate and that a unique preformed ice-binding structure in solution is not apparent. These observations do not support the rigid side chain model proposed recently by an X-ray study [Sicheri, F., & Yang, D. S. C. (1995) *Nature 375*, 427−431].

Fish antifreeze proteins (AFPs)[1] are a group of structurally diverse macromolecules that provide freeze resistance to teleost fish living in ice-laden marine environments (Davies & Hew, 1990). These proteins are present in millimolar concentrations in the serum and are able to depress the freezing point of the blood from −0.8 to about −2 °C. The depression of the freezing point is due to the ability of these proteins to inhibit ice crystal growth by binding to the ice surface, a process known as adsorption−inhibition (Raymond & DeVries, 1977). The adsorption of AFPs is thought to be site-specific. Ice etching studies support the hypothesis that most AFPs target and bind to defined ice lattice sites with specific orientations (Knight et al., 1991, 1993; Cheng & DeVries, 1991). The exact mechanism by which these proteins interact with the growing ice crystal remains unclear, although it is generally agreed that the protein binds ice by establishing a hydrogen-bonding network with the ice lattice through a good spatial match of its polar side chains to the ice surface water molecules.

At present, the best characterized and simplest fish antifreeze protein is the α-helical Type I AFP from the winter flounder (isoform HPLC-6) (Davies & Hew, 1990). It is a 37-amino acid, monomeric α-helical protein. The primary sequence of this protein and other Type I AFP isoforms is built of a tandemly repeated 11-amino acid unit. The repeat unit has the consensus sequence $TX_2N/DX_7$, where X is generally alanine. On the basis of modeling studies, it was first suggested by DeVries and Lin that the T and N/D residues reside on one face of the helix with an intraresidue (T−N/D) distance of 4.5 Å (DeVries & Lin, 1977). Since this matches the oxygen spacing of the water molecules on the prism face of the ice crystal, it was speculated that AFP binding occurred to the prism face. It was later revealed that Type I AFP binds selectively to the $\{2\ 0\ \bar{2}\ 1\}$ bipyramidal planes in the direction of $\langle 0\ 1\ \bar{1}\ 2\rangle$ (Knight et al., 1991). Therefore, it appears that the 16.5 Å spacing of the *i*,*i*+11 threonine residues is the critical feature since it matches the 16.7 Å distance of the water molecules on the adsorption plane. In contrast, the role of the asparagine or aspartate residues is less well established. Although they are placed along the helix with a spacing similar to that of the threonine residues, they are not conserved among Type I AFP (Davies & Hew, 1990). Furthermore, the carboxamide functional group differs from the hydroxyl in its H bond acceptor/donor capabilities. Recent models disagree on the exact role of these residues (Wen & Laursen, 1992; Chou, 1994; Madura et al., 1994; Sicheri & Yang, 1995).

The latest mechanism of action proposed for Type I AFP is derived from a well-resolved X-ray structure by Sicheri and Yang (1995). The protein possesses well-defined N- and C-cap structures which help explain the ability of the

[†] This work is supported by the Protein Engineering Network of Centres of Excellence of Canada and A/F Protein, Inc.

* Author to whom correspondence should be addressed.
[‡] Protein Engineering Network of Centres of Excellence, University of Alberta.
[§] Department of Biochemistry, University of Alberta.
[||] Case Western Reserve University.
[⊥] Queen's University.

[⊗] Abstract published in *Advance ACS Abstracts,* December 1, 1996.

[1] Abbreviations: AFP, antifreeze protein; TFA, trifluoroacetic acid; CD, circular dichroism; NMR, nuclear magnetic resonance; DQF-COSY, double-quantum filtered correlation spectroscopy; PE-COSY, primitive exclusive correlation spectroscopy; NOE, nuclear Overhauser effect; NOESY, nuclear Overhauser-enhanced spectroscopy.

S0006-2960(96)01934-4 CCC: $12.00 © 1996 American Chemical Society

protein to maintain its helicity. Each of the threonine residues adopted the same single rotameric conformation with $\chi_1$ near −60°. The side chains of N16 and N27 were also shown to be fixed due to van der Waals interaction with the *i,i*−4 leucines. These observations formed the basis of a rigid side chain ice binding model where the protein is envisioned to adsorb to ice via the constrained polar groups.

The constrained binding model proposed raises interesting issues concerning the flexibility of surface residues that are involved in molecular recognition. For Type I AFP, it might be advantageous to sacrifice side chain conformational entropy in favor of ice site recognition. However, given the small size of the protein, and the fact that the amino acids in question are surface residues, the entropic cost of fixing a conformation in solution is likely to be prohibitive in terms of protein stability. On the basis of this consideration, the side chain rotamer observed in the crystal might be only one of many conformations that the polar residues sample prior to ice binding.

Since the issue of side chain conformation is paramount to the understanding of the activity of AFPs, and the observations could be relevant to other systems where surface residues are involved in molecular recognition, the flexibility and mobility of the essential threonine, asparagine, and aspartate side chains in Type I AFP were investigated in this paper. Specifically, two-dimensional (2D) proton nuclear magnetic resonance experiments at low temperatures were performed. A combination of coupling constant measurements obtained from DQF- and PE-COSY experiments together with NOE data were used to determine the conformational state of the polar side chains.

## MATERIALS AND METHODS

*AFP Purification and Synthesis.* Synthetic HPLC-6 was synthesized with a solid-phase peptide synthesis methodology using a benzhydrylamine hydrochloride resin with conventional *N-tert*-butyloxycarbonyl (t-Boc) chemistry on an Applied Biosystems model 430A peptide synthesizer (Foster City, CA) as described (Hodges et al., 1988). Crude proteins were cleaved by a mixture of hydrogen fluoride [20 mL/(g of resin)], anisole (10%), and 1,2-ethanedithiol (2%) for 1.5 h at −5 °C and extracted with glacial acetic acid. Lyophilized acid extract was solubilized in 10% acetic acid, clarified by filtration through a 0.2 $\mu$m syringe filter, and applied onto a Synchropak RP-4 preparative C8 column (250 × 21.1 mm inside diameter, 6.5 $\mu$m particle size, and 300 Å pore size) (Synchrom, Lafayette, IN) controlled by a Beckman System Gold HPLC system (San Ramon, CA). The peptide was eluted by a linear AB gradient of 0.2% B/min at a flow rate of 5 mL/min, where solvent A was 0.05% trifluoroacetic acid (TFA) in water and solvent B was 0.05% TFA in acetonitrile. Purity of the protein was confirmed by reversed-phase analytical HPLC using a Zorbax SB 300 C8 column (250 × 4.6 mm inside diameter, 5 $\mu$m particle size, and 300 Å pore size) (Rockland Technologies, Wilmington, DE) on a Hewlett-Packard 1090 chromatograph with a liner AB gradient of 2% B/min and a flow rate of 0.25 mL/min. The identity and purity of the synthetic AFP were further analyzed by mass spectrometry and amino acid analysis. Electrospray mass spectrometry was performed using a Fisons VG Quattro mass spectrometer (VG Biotech, Cheshire, England). For amino acid analysis, proteins were hydrolyzed in 6 N HCl at 160 °C for 1.5 h in sealed evacuated tubes. The hydrolysate was analyzed in a Beckman model 6300 amino acid analyzer.

*Circular Dichroism Spectroscopy and Antifreeze Activity Measurement.* CD spectra were recorded on a Jasco J-500C spectropolarimeter (Jasco, Easton, MD). The instrument was calibrated with an aqueous solution of recrystallized *d*-10-(+)-camphorsulfonic acid at 290.5 nm. The temperature of the cuvette holder was maintained by a Lauda model RMS water bath (Brinkman Instruments, Rexdale, Ontario) using a 50/50 water/polyethylene glycol mixture as the coolant. Results were expressed as mean residue molar ellipticity [Θ] (deg cm$^2$ dmol$^{-1}$) calculated from the equation

$$[\Theta] = ([\Theta]_{obs}\mathrm{MRW})/(10lc) \quad (1)$$

where $[\Theta]_{obs}$ is the observed ellipticity expressed in millidegrees, MRW is the mean residue molecular weight (molecular weight of the protein divided by the number of amino acids), *l* is the optical path length in centimeters (0.05 cm), and *c* is the final protein concentration in milligrams per millilter. The change in helicity of the protein was monitored by collecting wave scans and in separate experiments by sampling data at 222 nm. For wave scans, CD spectra were the average of four scans obtained by sampling data at 0.1 nm intervals from 250 to 196 nm. For the temperature study which was monitored at 222 nm, the reported value at each temperature is the average of at least 32 samplings. The concentration of the synthetic protein was 0.47 mg/mL, and the buffer used for the temperature studies was 50 mM potassium phosphate and 50 mM KCl at pH 7.0.

*Activity Measurements.* The ability of the synthetic protein to depress the freezing point of a solution was assayed using a nanoliter osmometer (Clifton Technical Physics, Hartford, NY) by the method of Chakrabartty et al. (1991). The thermal hysteresis value (difference between the observed melting and freezing point of the solution) or activity was measured as a function of protein concentration in 0.1 M $NH_4HCO_3$ (pH 7.9).

*NMR Spectroscopy.* For the NMR experiments, 6.8 mg of the protein was dissolved in either 500 $\mu$L of $D_2O$ or 90% $H_2O$/10% $D_2O$ (v/v) to give 2 mM protein solutions. DDS (0.1 mM) was added for internal referencing. The pH of the two samples was adjusted to 7.0.

The 2D DQF-COSY, PE-COSY (Piantini et al., 1982; Rance et al., 1983; Müller, 1987), and NOESY spectra (Jeener et al., 1979; Macura & Ernst, 1980) were measured at 2 and 3 °C on a Varian Unity*plus* spectrometer operating at 600 MHz. For the DQF-COSY experiment at 3 °C using the 100% $D_2O$ sample, a sweep width of 6600 Hz in $F_2$ and of 3000 Hz in $F_1$ was used. The acquired data consisted of 2048 $F_2$ × 350 $F_1$ complex data points. The data were zero-filled to give a spectrum after transformation that contained 4096 × 2048 data points. For DQF-COSY experiments using the same sample at 2 °C, the sweep width was reduced to 800 Hz in $F_2$ and 3000 Hz in $F_1$. The acquired data consisted of 512 $F_2$ × 512 $F_1$ complex data points. The data were zero-filled to give a spectrum after transformation of 8192 × 8192 data points. The PE-COSY experiments were also performed on the $D_2O$ sample at 3 °C with a sweep width of 3000 Hz in both dimensions. The acquired data

consisted of 2048 $F_2 \times 350$ $F_1$ complex data points. The data were zero-filled to give a spectrum after transformation that contained 8192 × 4096 data points. Shifted sine bell window functions were applied in both dimensions for all the data mentioned here. The 2D NOESY spectra at 3 °C for the two samples were measured with a sweep width of 6600 Hz in $F_2$ and 3000 Hz in $F_1$ and a mixing time of 100 ms. The acquired data consisted of 2048 $F_2 \times 256$ $F_1$ complex data points. The data were zero-filled to give a spectrum after transformation that contained 4096 × 2048 data points.

All 2D DQF-COSY and NOESY spectra collected at a temperature of 6 °C were measured on a Varian Unity 500 spectrometer. For the 2D DQF-COSY spectra using the $D_2O$ sample, a sweep width of 833.3 Hz was used in $F_1$ and in $F_2$ with 512 complex data points in both dimensions. The spectra were processed with 4096 × 4096 data points using an unshifted sine bell window function in combination with line broadening in both dimensions. A baseline correction was not necessary. The 2D NOESY spectra on the same sample were measured using a sweep width of 6000 Hz in $F_1$ as well as in $F_2$ with a mixing time of 100 ms. The acquired data consisted of 1024 $F_2 \times 300$ $F_1$ complex data points. They were processed with 2048 × 2048 data points using shifted sine bell window functions in both dimensions. In $F_2$, an additional baseline correction was applied. No window functions were used in $F_2$, while a Gaussian and sine bell window function was applied in $F_1$. All spectra were referenced to the signals of the methyl groups of DSS (0.0 ppm).

*Determination of Coupling Constants and NOE Intensities.* In all cases, the $^3J_{\alpha\beta}$ coupling constants were determined from the peak separation of well-resolved DQF-COSY and/or PE-COSY multiplets. Curve fitting or related procedures were not necessary, due to the high digital resolution of the spectra. In the DQF-COSY spectrum at 6 °C for example, 512 complex data points were used for a sweep width of 833.3 Hz in both dimensions. The NOEs were integrated using the Varian VNMR processing software.

*Determination of $\chi_1$ Side Chain Torsion Angles.* The $\chi_1$ side chain torsion angles can be obtained by analyzing the pattern of $^3J_{\alpha\beta}$ coupling constants and the relative intensities of the intraresidue NOEs involving the Hα proton and the two H$\beta^{2,3}$ protons (Clore & Gronenborn, 1989; Karplus, 1959, 1963; Pardi et al., 1984; Montelione et al., 1989). Figure 1 outlines the information necessary to determine the $\chi_1$ angles for threonines. However, a side chain which is not fixed into one conformation will show an average coupling constant if the rotation is fast on the NMR time scale.

$$J_{\text{obs}} = \sum_i P_i J_i \qquad (2)$$

$P_i$ corresponds to the fractional occupancy of a conformation corresponding to the coupling constant $J_i$. On the basis of the expected coupling constants for the different rotamers, it is then possible to calculate the occupancy of a specific rotamer from a measured coupling constant and vice versa. For a threonine side chain that has no preference, a coupling constant of 6.6 Hz would be obtained (Figure 1 and eq 2).

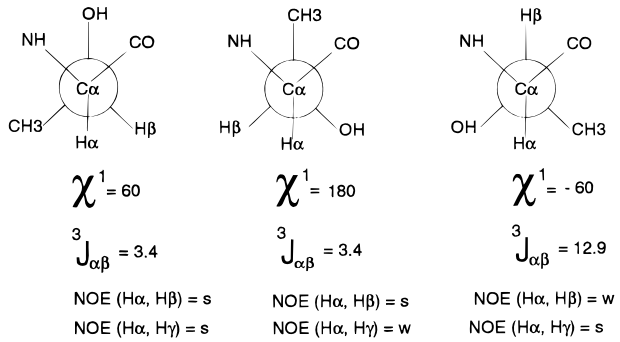


FIGURE 1: Correlation between $^3J_{\alpha\beta}$ NMR coupling constants and corresponding NOE intensities with $\chi_1$ side chain torsional angles for the three most populated rotamer conformations of threonine. The molecules are shown in the Newman projection with the Cα in the front and the C$\beta$ in the back. For each of the three expected $\chi_1$ values, the corresponding coupling constants and NOE intensities are given using a distance classification of ≤2.7 and ≤5 Å for strong and weak NOEs, respectively. The expected distances were derived from an analysis of 20 crystal structures (Nilges et al., 1990).

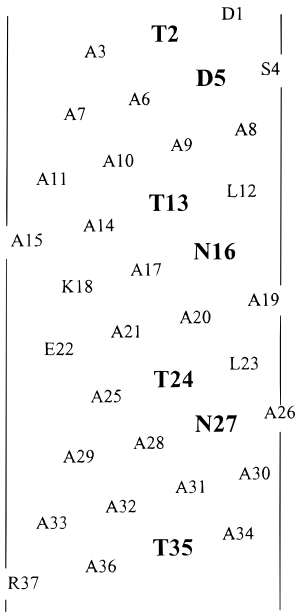


FIGURE 2: Helical net representation of the Type I AFP sequence. The threonine, asparagine, and aspartate residues implicated in ice binding are highlighted.

## RESULTS

The amino acid sequence of the synthetic Type I AFP is shown in Figure 2. The polar residues implicated in ice binding (threonine, asparagine, and aspartate) are highlighted. The synthetic protein is amidated at the C terminus as is the native protein. Figure 3 displays the CD spectra of the helical protein obtained at various temperatures. The change in helicity as a function of temperature was also monitored by the change in ellipticity at 222 nm (Figure 3, inset) in a separate experiment. The protein undergoes a helix−coil transition identical to that of the natural AFP (data not shown). About 50% of the helicity observed at 0 °C was lost around 22 °C. The protein was fully denatured near 60 °C. Under these experimental conditions, the helix−coil transition is fully reversible. On the basis of the 222 nm ellipticity value at 0 °C (Figure 3, inset), the protein adopts a full helical conformation near the freezing temperature of water. Sedimentation equilibrium ultracentrifugation experiments indicated that the protein remains monomeric under

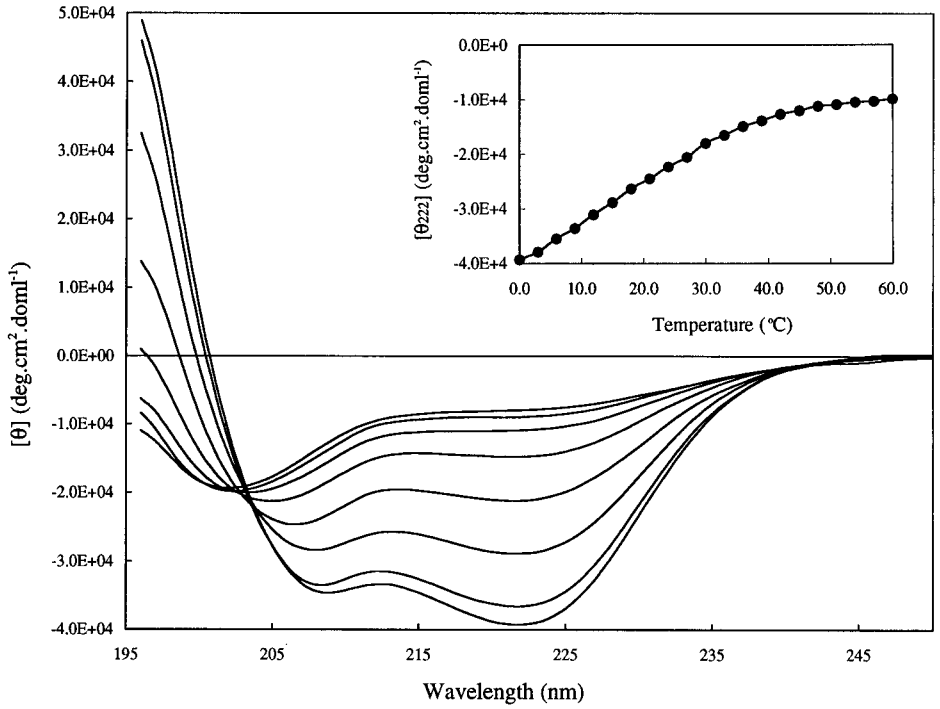


FIGURE 3: Thermal denaturation profile of the Type I AFP as monitored by circular dichroism. Spectra (196−250 nm) were collected at 5 °C intervals starting at 1 °C and ending at 65 °C. The spectra displayed are those collected at (from bottom to top) 1, 5, 15, 25, 35, 45, 55, and 65 °C. (Inset) In a separate experiment, the dependence of the molar residual ellipticities at 222 nm on temperature was also studied. The thermal denaturation profile of Type I AFP is fully reversible under the present conditions.

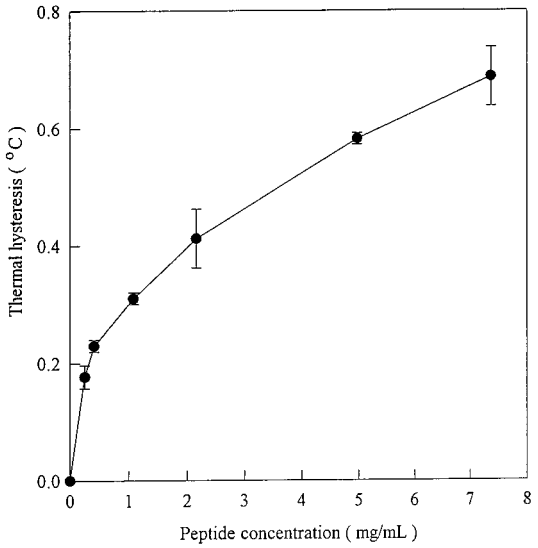


FIGURE 4: Thermal hysteresis activity as a function of the synthetic AFP concentration. Each point is the average of three to five determinations. Standard deviations are shown by the vertical bars.

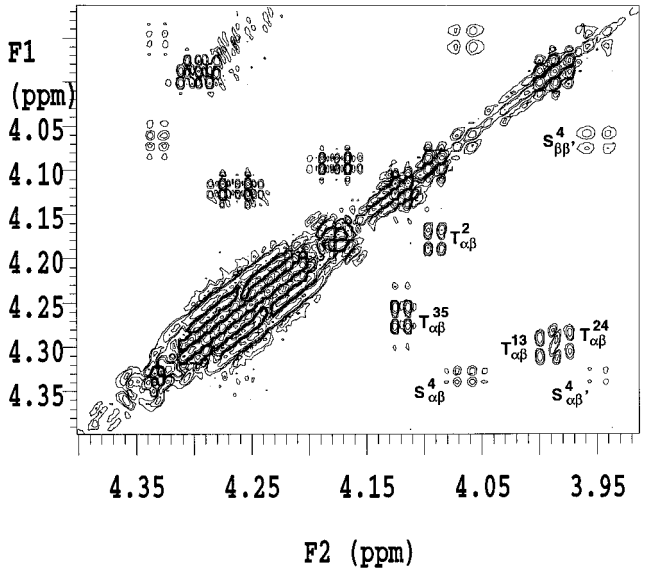


FIGURE 5: 2D DQF-COSY $^1$H NMR spectrum of Type I AFP at 3 °C in $D_2O$. The H$\alpha$−H$\beta$ region containing cross-peaks from T2, S4, T13, T24, and T35 is displayed.

these conditions (data not shown). The synthetic protein is fully active and able to bind ice. The depression of the freezing point as a function of protein concentration (Figure 4) was similar to that observed for the native protein (Scott et al., 1987).

NMR spectroscopic characterization of the antifreeze protein began with the sequential assignment of the protein using a combination of 2D NOESY and DQF-COSY experiments. For the assignment, mostly $d_{NN}(i,i\pm1)$, $d_{\alpha N}(i,i+1)$, $d_{\alpha N}(i,i+3)$, and $d_{\alpha\beta}(i,i+3)$ NOEs were used in a standard strategy (Wüthrich, 1986). It was possible to obtain assignments for all of the hydrophilic and several nonpolar residues. For the threonines, the H$\alpha$ and H$\beta$ cross-peaks were readily identified in the DQF-COSY spectrum (Figure 5). The lack of aromatics and glycines and the presence of only one serine in the primary sequence of Type I AFP enable the unambiguous assignment of all four threonines (Figure 5). However, it was not possible to sequentially assign all of the alanines due to signal overlap. A summary of the observed chemical shifts for the various hydrophilic side chains at 3 °C is presented in Table 1. The NH chemical shifts were obtained from a NOESY spectrum measured at 3 °C using the 90% $H_2O$ sample, while the remaining data were obtained from the 100% $D_2O$ sample examined under similar conditions. There was no observable difference between the chemical shifts obtained from the $D_2O$ or the

Table 1: Chemical Shifts and Coupling Constants of Selected Polar Residues in Type I AFP

| residue | $\delta$NH (ppm)[a] | $\delta$H$\alpha$ (ppm) | $\delta$H$\beta$ (ppm) | $\delta$H$\beta'$ (ppm) | $^3J_{\alpha\beta}{}^2$ (Hz) | $^3J_{\alpha\beta}$ (Hz) | $\Delta\delta$H$\alpha$ (ppm)[b] | type[c] |
|---|---|---|---|---|---|---|---|---|
| D1 | − | 4.30 | 3.20 | 2.96 | 5.0 | 5.2 | −0.46 | PE |
| D5 | 8.52 | 4.51 | 2.87 | 2.72 | 9.2 | 4.4 | −0.25 | PE |
| S4 | 8.83 | 4.32 | 4.05 | 3.94 | 4.6 | 4.0 | −0.24 | PE |
| N16 | 8.75 | 4.59 | 2.98 | 2.85 | 8.4 | 4.5 | −0.16 | PE |
| N27 | 8.73 | 4.59 | 2.98 | 2.85 | 8.4 | 4.5 | −0.16 | PE |
| T2 | − | 4.09 | 4.17 | − | 7.1 | − | −0.26 | DQF |
| T13 | 8.28 | 3.97 | 4.29 | − | 8.5 | − | −0.38 | DQF |
| T24 | 8.30 | 3.97 | 4.29 | − | 8.5 | − | −0.38 | DQF |
| T35 | 8.10 | 4.11 | 4.26 | − | 6.8 | − | −0.24 | DQF |

[a] $\delta$NH chemical shifts were obtained from a NOSEY spectrum obtained at 3 °C using the 10% $D_2O$ sample. [b] $\Delta\delta$H$\alpha$ are the α-proton chemical shift differences between measured shifts and standard values (Wüthrich, 1986). [c] Experiment types from which the coupling constants other than the $\delta$NH values were obtained.

$H_2O$ sample. The complete chemical shift data are given as Supporting Information.

The well-resolved DQF-COSY cross-peaks permitted the determination of the $^3J\alpha\beta^2$ coupling constant for each threonine. It is important to note that the coupling constants observed did not change significantly (<0.3 Hz) when varying the temperature between 2 and 6 °C. A summary of all the observed coupling constants for the various hydrophilic side chains at 3 °C is presented in Table 1. The observed $^3J_{\alpha\beta}{}^2$ coupling constants for the four threonines do not correspond to any one of the three known rotamers (Figure 1); instead, they correspond to an average of more than one conformation (eq 2). The same observations were made for D5, N16, and N27. However, D1 and S4 exhibit a strong preference for the $\chi_1 = +60°$ rotamer. This is probably due to their involvement in the N-cap structure (Sicheri & Yang, 1995).

The accuracy of the observed experimental coupling constants for the threonine residues in the antifreeze protein has been evaluated by comparing the observed $^3J_{\beta\gamma}$ coupling constant obtained for the free amino acid in solution with its theoretically expected value. This coupling constant was chosen because we can assume the methyl group rotates freely. Under these circumstances, a $^3J_{\beta\gamma}$ coupling constant of 6.6 Hz is expected. On the basis of the DQF-COSY spectrum of threonine in water at 6 °C obtained under similar conditions used for the antifreeze studies (Figure 6), the observed coupling constant was 6.82 Hz, which is only 0.22 Hz larger than the expected theoretical value. This result places the upper limit of the error of measurements at around 0.3 Hz. This is due to the high digital resolution of the DQF-COSY spectrum which allows a precise evaluation of the coupling constants. Comparison of Figure 6 with Figure 5, which shows the H$\alpha$−H$\beta$ cross-peaks for the four threonines in Type I AFP, shows no significant decrease in spectra quality owing to line broadening by going from the free amino acid to the full protein. Furthermore, line broadening would only increase the observed coupling constants, and the maximum observed coupling constant for the threonines is 8.5 Hz. For a fixed side chain conformation with a $\chi_1$ of −60° as observed for the X-ray structure, a coupling constant of 12.9 Hz would be expected. Therefore, even with a small overestimation of the measured coupling constants, the results demonstrate that the threonine side chains do not adopt a fixed conformation.

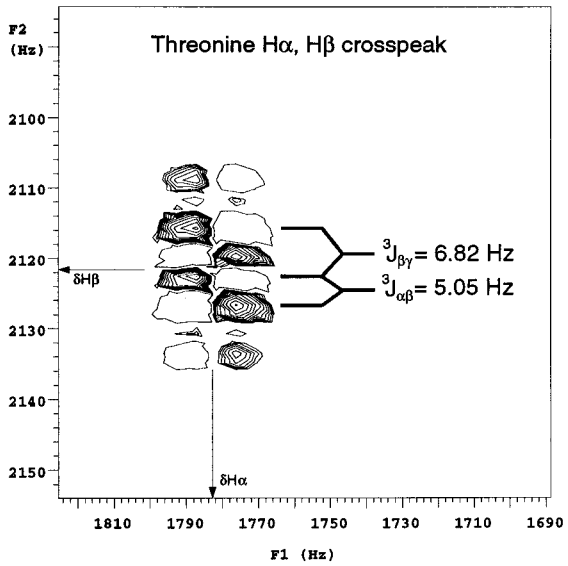


FIGURE 6: 2D DQF-COSY $^1$H NMR spectrum of 5 mM threonine at 6 °C and 100% $D_2O$. The region containing the H$\alpha$−H$\beta$ cross-peak pattern is displayed to show the fine splitting of that cross-peak. To distinguish between positive and negative peaks, negative peaks are displayed as open circles.

Table 2: NOE Ratio of the Threonine Residues

| residue | T2[a] | T13 | T24 | T35[a] |
|---|---|---|---|---|
| ratio | − | 0.91 | 0.91 | − |

[a] The H$\alpha$−H$\beta$ cross-peaks of T2 and T35 were too close to the diagonal to be resolved, so no NOE ratios are reported.

In addition to information obtained from coupling constant measurements, the preferred rotameric state of the threonines was also assessed by analyzing the NOE information of the α-, $\beta$-, and $\gamma$-protons in the form of NOE ratios. The NOE ratio is defined according to the following formula:

$$\text{ratio} = \frac{(\text{NOE}_{\text{H}\alpha-\text{H}\beta})}{1/3(\text{NOE}_{\text{H}\alpha-\text{H}\beta})} \qquad (3)$$

The H$\alpha$−H$\gamma$ NOE in the above formula was divided by 3 to take into account the three threonine methyl protons when compared to the one $\beta$−proton. As shown in Figure 1, a NOE ratio significantly larger than 1 corresponds to a $\chi_1$ of 180°, while a NOE ratio significantly less than 1 corresponds to a $\chi_1$ of −60°. NOE ratios of around 1, as were obtained for T13 and T24 (Table 2), correspond either to a $\chi_1$ of 60° or to a free-rotating side chain. The proximity of the T2 and T35 H$\alpha$−H$\beta$ cross-peaks to the diagonal did not allow the evaluation of NOE ratios for these residues.

In order to assess the stability of the helix, and its influence on the flexibility of the threonine side chains, the α-proton chemical shift of observable residues was measured and compared to standard values (Wüthrich, 1986). It has been shown that the α-proton chemical shifts are dependent on the nature and character of the protein secondary structure (Wishart et al., 1992), such that upfield shifts relative to the random coil values are found for residues in α-helices and downfield shifts are observed for those residues in $\beta$-sheets. For all assigned residues, the α-proton chemical shifts indicate a stable helical environment for the whole protein (Table 1). None of the observed residues populated the $\beta$ or the random conformation in any significant proportion.

Due to the N- and C-cap structures, even the residues at the N- and C-terminal ends adopted a stable helical structure. A comparison of the α-proton chemical shifts for the four threonines alone suggests that the two central threonines (T13 and T24) may experience a slightly less dynamic environment as indicated by the smaller chemical shift value.

The helical state of the protein can further be assessed from a study of the $d_{NN}(i,i+1)$ and $d_{\alpha N}(i,i+3)$ NOEs. In general, values typical of a helical backbone were found for residues starting from T2 and ending at A31 (data not shown), in agreement with the α-proton chemical shifts values. Unfortunately, quite a few NOEs are unresolved, especially for the region from A32 to R37, due to significant signal overlap. Nonetheless, it is reasonable to suggest that on the basis of the α-proton chemical shifts (Table 1) and the NOE data (data not shown) the entire protein adopts a helical conformation in solution under the conditions employed for the NMR studies.

## DISCUSSION

The ability of fish antifreeze proteins to bind ice has been known for over two decades (Cheng & DeVries, 1991; Davies & Hew, 1990). However, the molecular mechanism by which these proteins adsorb to ice remains elusive. The inability to observe the interaction of protein and ice at the molecular level has hampered the development of a satisfactory ice-binding mechanism. So far, most hypotheses rely on two basic assumptions. The first one is that the antifreeze adsorbs to ice via hydrogen bonds, and the second premise is that this H-bonding network is provided through surface accessible polar groups that are uniquely arranged. The high-resolution X-ray structure of the α-helical Type I AFP (Sicheri & Yang, 1995) provides experimental support for the latter assumption. It shows that the ice-binding residues of Type I AFP are strategically arranged on one face of the helix in almost linear arrays (Figure 2). Additionally, the threonines, asparagines, and aspartate are spaced precisely to interact with the identified ice plane (Sicheri & Yang, 1995), which supports the hypothesis that AFP binds ice through a lattice-matching mechanism.

In order to understand the molecular mechanism of ice binding, the characterization of the critical side chain conformations is necessary. In Figure 1, the expected $^3J_{\alpha\beta}{}^2$ coupling constants are shown for the three most commonly observed threonine side chain rotamers. A side chain which is not fixed into one of these conformations, but instead rotates between them, will show an average coupling constant if the rotation is fast on the NMR time scale. On the basis of the expected values for the different rotamers, it is possible to calculate the occupancy of a specific rotamer from a measured coupling constant (eq 2). The measured $^3J_{\alpha\beta}{}^2$ coupling constants of 7.1 and 6.8 Hz for T2 and T35 are very close to the expected value of 6.6 Hz for an unrestricted side chain, where all three rotamers are equally populated. For the side chains of T13 and T24, which are in the center of the helix, a coupling constant of 8.5 Hz is observed. In the following equation, $P_1$, $P_2$, and $1 - P_1 - P_2$ describe the amount of time the side chain stays in the 60, 180, and −60° conformation.

$$8.5\ \text{Hz} = P_1 \times 3.4\ \text{Hz} + P_2 \times 3.4\ \text{Hz} + (1 - P_1 - P_2) \times 12.9\ \text{Hz} \quad (4)$$

Solving this equation shows that the side chains of T13 and T24 do populate, on average, the $\chi_1 = -60°$ conformation around 55% of the time.

The flexible picture presented by the coupling constant measurements is further corroborated by an analysis of the NOE ratio (eq 3) of the threonines. Figure 1 gives the expected NOE values for the three common threonine side chain rotamers. As described for the coupling constants, a rotating side chain will lead to an averaging of the observed NOE values. If the distribution of rotameric populations of this residue is close to random, a ratio of the NOE signal intensities of the Hα−H$\beta$ atoms to the Hα−H$\gamma$/3 atoms would be close to unity (Figure 1). As presented in Table 2, the side chains of T13 and T24 are indeed shown to be mobile. Unfortunately, the proximity of the Hα−H$\beta$ cross-peaks for T2 and T35 to the diagonal prevented a formal analysis by this method for these residues.

The side chains of N16 and N27 are shown to be mobile in solution, despite the close proximity of the asparagine and leucine side chains as indicated by the presence of NOE cross-peaks (data not shown). From PE-COSY experiments, the $^3J_{\alpha\beta}{}^2$ and $^3J_{\alpha\beta}{}^3$ coupling constants were 8.4 and 4.5 Hz, respectively, for both N16 and N27. In a manner similar to that for the threonines, it is possible to calculate the populations for the different rotamers from the coupling constants. Since two coupling constants are available, it is possible to calculate the average population for the three rotamers. As described for T13 and T24 (eq 4), we can write the following equation for $^3J_{\alpha\beta}{}^2$:

$$8.4\ \text{Hz} = P_1 \times 3.4\ \text{Hz} + P_2 \times 3.4\ \text{Hz} + (1 - P_1 - P_2) \times 12.9\ \text{Hz} \quad (5)$$

For $^3J_{\alpha\beta}{}^3$

$$4.5\ \text{Hz} = P_1 \times 3.4\ \text{Hz} + P_2 \times 12.9\ \text{Hz} + (1 - P_1 - P_2) \times 3.4\ \text{Hz} \quad (6)$$

Solving eq 5 shows that the side chains spend 53% of their time in the $\chi_1 = -60°$ conformation. Equation 5 can than be rearranged to express $P_1$ in terms of $P_2$ and can be combined with eq 6 to give $P_2$ which corresponds to the $\chi_1 = 180°$ rotamer. This is the least populated rotamer, with the side chains adopting this conformation around 10% of the time. For the remaining 37% of the time, the side chains will adopt the next rotamer with a $\chi_1$ of 60°. These data show clearly that the side chains of N16 and N27 are not restrained in solution, in contrast to a fixed $\chi_1$ of −75° observed in the crystal (Sicheri & Yang, 1995). Therefore, the proposed role of L12 and L23 as critical stabilizers for the N residues prior to ice binding is also called into question. However, the present data set cannot rule out the possibility that, after the initial ice site recognition, the leucine residues might enhance the overall binding affinity by helping to stabilize the asparagine side chain in its ice-bound form through van der Waals contacts. The same type of calculations was performed for D5. Here, the side chain adopts the $\chi_1 = -60°$ rotamer 60% of the time and the $\chi_1 = 180°$ rotamer 11% of the time and the remaining 28% of the time is spent in the $\chi_1 = 60°$ conformation.

The NMR analyses of Type I AFP at low temperatures indicate that the critical polar residues are mobile and dynamic during their search for the ice-binding site. This

provides an alternative picture to the rigid and restrained model based on X-ray data (Sicheri & Yang, 1995). The observed −60° rotamer of the threonine side chain in the crystal state is apparently only one of the many conformations that is observed in solution. The preformation of a unique ice-binding structure in solution is not evident.

Since the threonine side chain in Type I AFP is mobile in solution, it is not necessary to conform an ice-binding mechanism to a hypothesis based on the −60° rotamer observed in the crystal state. If the hydroxyl of the threonine residue is critical in the ice-binding event, the −60° rotamer might in fact be a poor candidate for ice binding. In this conformation, the HG1 atom of the hydroxyl is about 2 Å away from the O atom of the *i*,*i*−4 alanine residue and forms an angle of roughly 158°. Therefore, the hydroxyl is positioned almost ideally to form a hydrogen bond with the backbone carbonyl. The potential of forming this H bond is likely to explain why the −60° conformation is observed to 85% in α-helices in crystal structures, while the 60 and 180° conformations are observed to 13 and 2%, respectively (McGregor et al., 1987; Schrauber et al., 1992). This explains as well why the −60° conformation is observed to some extent in solution as demonstrated here. Modeling studies (data not shown) clearly showed that the threonine side chains can adopt all three different rotamers without experiencing steric clashes. When the threonine residue is presented with an ice surface which is a network of relatively stable H bond partners, it might be energetically more favorable for the hydroxyl to interact with the ice layer in conformations where it can serve as a proton donor and an acceptor. Therefore, in the development of a rigorous mechanism of action for Type I AFP, it is important to consider the flexibility of the polar side chains and their potential to search for an optimal H-bonding arrangement within the confines of the structural steric constraints.

From the NMR analyses, it is envisioned that the conformation of the ice-binding side chains becomes less mobile only after a stable H-bonding network is established with the ice surface. Since the identified ice adsorption plane for Type I AFP has a characteristic 16.7 Å oxygen repeat spacing (Knight et al., 1991), it is assumed that, once the protein is stably bound on ice, the ice-binding residues will adopt a similar rotameric form to maintain a spatial match with the ice layer. This "coalescence" model is akin to the "induced-fit" concept rather than to the "lock and key" description as far as the conformation of the polar side chains is concerned. However, the initial flexibility of the side chain is not to be confused with a loss in specificity, since the latter is dictated at least by the global arrangement of all ice-binding residues and not by the individual H-bonding group.

## ACKNOWLEDGMENT

We thank Bruce Lix and Gerry McQuaid for NMR upkeep, Paul Semchuk, Iain Wilson, and Leonard Daniels in the peptide synthesis and mass spectrometry laboratory, the Alberta Peptide Institute for amino acid analysis, Bob Luty for CD spectroscopy, Dr. Robert S. Hodges for helpful discussions, and Michele Loewen for antifreeze activity measurements.

## SUPPORTING INFORMATION AVAILABLE

$^1$H chemical shifts and assignments for Type I AFP at pH 7.0 and 3 °C (1 page). Ordering information is given on any current masthead page.

## REFERENCES

Charkrabartty, A., & Hew, C. L. (1991) *Eur. J. Biochem. 202*, 509−517.
Cheng, C. C., & DeVries, A. L. (1991) in *Life Under Extreme Conditions* (di Prisco, G., Ed.) pp 1−14, Springer-Verlag, Berlin.
Chou, K. C. (1994) *J. Mol. Biol. 223*, 509−517.
Clore, G. M., & Gronenborn, A. M. (1989) *Crit. Rev. Biochem. Mol. Biol. 24*, 479−557.
Davies, P. L., & Hew, C. L. (1990) *FASEB J. 4*, 2460−2468.
DeVries, A. L., & Lin, Y. (1977) *Biochim. Biophys. Acta 495*, 388−392.
Hodges, R. S., Semchuk, P. D., Taneja, A. K., Kay, C. M., Parker, J. M. R., & Mant, C. T. (1988) *Peptide Res. 1*, 19−30.
Jeener, J., Meier, B. H., Bachmann, P., & Ernst, R. R. (1979) *J. Chem. Phys. 71*, 4546−4553.
Karplus, M. (1959) *J. Chem. Phys. 10*, 11−15.
Karplus, M. (1963) *J. Am. Chem. Soc. 85*, 2870−2871.
Knight, C. A., Cheng, C. C., & DeVries, A. L. (1991) *Biophys. J. 59*, 409−418.
Knight, C. A., Driggers, E., & DeVries, A. L. (1993) *Biophys. J. 64*, 252−259.
Macura, S., & Ernst., R. R. (1980) *Mol. Phys. 41*, 95−117.
Madura, J. D., Wierzbicki, A., Harrington., J. P., Maughton, R. H., Raymond, J. A., & Sikes, C. S. (1994) *J. Am. Chem. Soc. 116*, 417−418.
McGregor, M. J., Islam, S. A., & Sternberg, M. J. E. (1987) *J. Mol. Biol. 198*, 295−310.
Montelione, G. T., Winkler, M. E., Rauhenbuehler, P., & Wagner, G. (1989) *J. Magn. Reson. 44*, 198.
Müller, L. (1987) *J. Magn. Reson. 72*, 191.
Nilges, M., Clore, G. M., & Gronenborn, A. M. (1990) *Biopolymers 29*, 813−822.
Pardi, A., Billeter, M., & Wüthrich, K. (1984) *J. Mol. Biol. 180*, 741−775.
Piatini, U., Sørensen, O. W., & Ernst, R. R. (1982) *J. Am. Chem. Soc. 104*, 6800−6801.
Rance, M., Sørensen, O. W., Bodenhausen, G., Wagner, G., Ernst, R. R., & Wüthrich, K. (1983) *Biochem. Biophys. Res. Commun. 117*, 479−485.
Raymond, J. A., & DeVries, A. L. (1977) *Proc. Natl. Acad. Sci. U.S.A. 74*, 2589−2593.
Raymond, J. A., Wilson, P., & DeVries, A. L. (1989) *Proc. Natl. Acad. Sci. U.S.A., 86*, 881−885.
Schrauber, H., Eisenhaber, F., & Argos, P. (1993) *J. Mol. Biol. 230*, 592−612.
Scott, G. K., Davies, P. L., Shears, M. A., & Fletcher, G. L. (1987) *Eur. J. Biochem. 168*, 629−633.
Sicheri, F., & Yang, D. S. C. (1995) *Nature 375*, 427−431.
Wen, D., & Laursen, R. A. (1992) *Biophys. J. 63*, 1659−1662.
Wishart, D. S., Sykes, B. D., & Richards, F. M. (1992) *Biochemistry 31*, 1647−1651.
Wüthrich, K. (1986) *NMR of Proteins and Nucleic Acids*, Wiley, New York.

BI961934W